PLANT SCIENCE TODAY
Vol x(x): xx–xx
https://doi.org/10.14719/pst.9249

eISSN 2348-1900

RESEARCH ARTICLE

Unveiling the antioxidant potential of *Curcuma amada* Roxb. leaf essential oil : An *in silico* and *in vitro* investigation of major constituents

Arpita Priyadarshini, Debajani Mohanty, Ambika Sahoo, Biswabhusan Dash, Pratap Chandra Panda, Sanghamitra Nayak, Asit Ray* & Sudipta Jena*

Centre for Biotechnology, Siksha O Anusandhan (Deemed to be University), Kalinga Nagar, Bhubaneswar 751 003, Odisha, India

*Correspondence email - sudiptajena@soa.ac.in; asitray@soa.ac.in

Received: 02 May 2025; Accepted: 18 July 2025; Available online: Version 1.0: 21 August 2025

Cite this article: Priyadarshini A, Mohanty D, Sahoo A, Dash B, Panda PC, Nayak S, Ray A, Jena S. Unveiling the antioxidant potential of *Curcuma amada* Roxb. leaf essential oil: An *in silico* and *in vitro* investigation of major constituents. Plant Science Today (Early Access). https://doi.org/10.14719/pst.9249

Abstract

Elevated levels of human peroxiredoxin 5 (Prdx5), a cytoprotective antioxidant enzyme protects cellular compartments from oxidative damage induced by peroxides. In recent years, essential oils are regarded a viable source of non-toxic antioxidant substances with a higher safety profile. *Curcuma* species have been shown to inhibit lipid peroxidation levels and enhance antioxidant enzyme activities. Thus, the present study was designed to screen potential antioxidant agents from *C. amada* leaf essential oil (CALEO) to interact and support the Prdx5 enzyme activity using *in vitro* and computational approaches. The essential oil obtained from was chemically characterised using GC-MS. The analysis identified 36 constituents with camphor (17.51 %), spathulenol (12.00 %) and curdione (10.27 %) as the major constituents of CALEO. Moreover, the antioxidant effects of the oil were evaluated using 2,2-diphenyl-1-picrylhydrazyl (DPPH) and 2,2'-azino-bis (3-ethylbenzothiazoline-6-sulfonic acid) (ABTS) free radical scavenging assays, in which it demonstrated high DPPH (IC_{50}= 6.91 ± 0.04 µg/mL) and ABTS (IC_{50}= 5.86 ± 0.06 µg/mL) radical scavenging effects as compared to positive control. Subsequently, molecular docking analysis was carried out between the key compounds of CALEO and Prdx5 protein. Amongst all, β-caryophyllene, germacrone and ar -turmerone exhibited strong binding affinity (< -5.8 kcal/mol) against Prdx5 as compared to ascorbic acid (-5.3 kcal/mol). Furthermore, molecular dynamics parameters such as RMSD (root mean square deviation), RMSF (root mean square fluctuation), Rg (radius of gyration), solvent accessible surface area (SASA), secondary structure and intermolecular H-bond plotted for the top scoring docked molecules indicated stability and minimal-fluctuations over a 100 ns simulation period. Molecular mechanics poisson-boltzmann surface area (MM/PBSA) analysis revealed that Vander Waals interactions were the major contributor for stabilizing the complexes. Additionally, chemical absorption-distribution-metabolism-excretion-toxicity (ADMET) analysis was conducted that revealed favourable pharmacokinetic and toxicity profiles for the lead compounds. Density functional theory (DFT) analysis was performed to investigate global reactivity parameters including MEP (molecular electrostatic potential), ELF (electron localization function), LOL (local orbital locator) and NCI-RDG (non-covalent interactions-reduced density gradient) for β-caryophyllene, germacrone, ar-turmerone and ascorbic acid. Ar-turmerone and germacrone displayed a small energy gap and higher reactivity compared to ascorbic acid. These findings suggest that germacrone and ar-turmerone may serve as promising novel antioxidant agents.

Keywords: ADMET; *Curcuma amada*; DFT; human peroxiredoxin-5; MD simulation; molecular docking

Introduction

Oxidative stress plays a major role in the pathogenesis and pathophysiology of several ailments, such as autoimmune diseases, cancer, rheumatoid arthritis, aging, neurological and cardiovascular disorders. It is primarily associated with the accumulation of excessive reactive oxygen/reactive nitrogen species (ROS/RNS) (1-3). Exposure to ROS/RNS leads to adverse effects such as enzyme-inhibition, lipid peroxidation and deoxyribonucleic acid (DNA) damage, which can ultimately affect the growth, metabolism, differentiation and motility of normal cells (4). Antioxidant defence proteins such as peroxiredoxin, superoxide dismutase (SOD), catalase and DT-diaphorase have been reported to protect the body from ROS/RNS and peroxide induced cellular damage (5, 6).

Among the six mammalian peroxiredoxins, Prdx5 is unique due to its atypical 1-cys peroxidase mechanism and its distribution across multiple cellular compartments, including mitochondria, peroxisomes and the cytosol (7). This broad localization allows Prdx5 to act as a crucial defender against ROS in diverse microenvironments. Prdx5 functions as mammalian thioredoxin peroxidase, facilitating the reduction of alkyl hydroperoxides, hydrogen peroxide and peroxynitrite, thereby reducing the harmful effects of ROS within the cells (8). Moreover, Prdx5 has been implicated in modulating inflammatory responses and cell survival under oxidative stress conditions, making it an attractive target for investigating novel antioxidant therapeutics. Prdx5 has been identified as a potential contributor to chemoresistance against vinblastine, dacarbazine, bleomycin and adriamycin in patients diagnosed with hodgkin's lymphoma,

likely by interfering with chemotherapeutics-mediated apoptosis. Furthermore, elevated expression of Prdx5 has also been detected in the thyroid tissues of individuals with Grave's disease, suggesting its involvement in disease progression.

In certain types of cancer such as gastric cancer, non-small cell lung cancer and breast cancer-Prdx5 has been shown to promote metastasis, highlighting its malignant potential. Modern pharmacological treatments involving the ubiquitous use of synthetic antioxidants such as butylated hydroxyl anisole (BHA), butylated hydroxy toluene (BHT) for oxidative stress have proven to be effective but are associated with several side effects under the influence of several mechanisms (9). Previous studies have associated BHA with the impairment of mitochondrial functions specifically through the inhibition of ATP-dependent biosynthetic pathways and ammonia detoxification processes, thereby, leading to an increased production of ROS within the cells. Similarly, BHT has exhibited concerning biological effects; its quinone methylation (QM) derivatives can form covalent adducts with key protective enzymes in the lungs, including glutathione S-transferase (GST) and SOD, thereby contributing to the accumulation of oxidative species.

Elevated ROS levels further might interact with regulatory protein such as *Keap1* and might disrupt the *Nrf2-ARE* signalling pathway. Dysregulation of this pathway might lead to a cellular microenvironment that may induce tumor progression. Consequently, there is increasing demand for natural antioxidant agents in the pharmaceutical industry. Essential oils are considered as feasible alternative source of non-toxic antioxidant compounds with a better safety profile.

Curcuma amada Roxb. (mango ginger), an aromatic, rhizomatous medicinal plant of the Zingiberaceae family, has garnered interest due to its bioactive constituents and therapeutic properties (10). It is mainly found in the Indo-Malayan region, Africa, Australia and tropical Asia (11). The plant has been reported to exhibit antitumor, antibacterial, antidiabetic, anti-inflammatory, anti-obesity, CNS (central nervous system) depressant, enterokinase inhibitory properties, antiallergic, platelet aggregation inhibitory and antioxidant properties (12). *Curcuma* species including *C. caesia* and *C. longa* have also been shown to inhibit the level of lipid peroxidation and enhance the antioxidant enzyme activity in *in vitro* and *in vivo* models (13, 14).

Considering the abundance of research reports on the antioxidant effects of *Curcuma* essential oils, the current study aimed to screen bioactive constituents from *C. amada* leaf essential oil (CALEO) with potential as novel antioxidants for mitigating oxidative stress. The major constituents of CALEO were identified through GC-MS analysis. Molecular docking studies were conducted to assess the interaction between the active components of CALEO with the human target protein peroxiredoxin 5 (Prdx5), an antioxidant enzyme.

Additionally, molecular dynamics (MD) simulation and MM/PBSA analysis were performed to evaluate the flexibility and stability of complexes formed between Prdx5 and the top-docked CALEO compounds, revealing any structural or functional changes during the binding process. *In-silico* ADME/T analysis was also carried out on the screened compounds to determine their drug-likeness, pharmacokinetics and toxicity. Furthermore, density functional theory (DFT) calculations were performed to identify the reactive nature, potential specific reactive sites, stable molecular structures and bonding patterns of the major lead compounds. The detailed workflow of the study is depicted in Supplementary Fig. SF1.

Materials and Methods

Plant material collection and isolation of essential oil

Fresh leaves of *C. amada* were collected from Aiginia, Khurda, Odisha (20°14'51.1"N, 85°46'49.4"E) in November 2023. The plant sample was verified by Prof. Pratap Chandra Panda and the voucher specimen (2550/CBT/Dt. 23.11.2023) was deposited in the herbarium of Centre for Biotechnology, SOA (Deemed to be University), Bhubaneswar, Odisha. Fresh leaves (500 g) were hydro-distilled for 6 hr using the procedure described in the European Pharmacopoeia (15). The obtained essential oil was dehydrated using anhydrous sodium sulphate to remove traces of water and then stored at 4 °C for further analysis.

Chemical characterization of leaf essential oil

The chemical characterization of the leaf oil was performed on a Clarus-580 gas chromatograph (Perkin Elmer, USA) fitted with an SQ-8 MS detector. 0.1 µL of sample was injected in split less mode and separated on an Elite-5 MS capillary column (30 m × 0.25 mm, 0.25 µm thickness). Helium was used as the carrier gas at a flow rate of 1 mL/min. The temperature of the oven was initially set at 60 °C, then increased to 220 °C at a rate of 3 °C/min and held at the same temperature for 7 min. The ionization energy was adjusted to 70 eV. The injector and source temperature were set at 250 °C and 150 °C, respectively. The identification of each compound in the leaf essential oil was detected by comparing the mass spectra of the compounds with the spectra available in the NIST (National Institute of Standards and Technology) library. Only compounds with a match quality greater than 90 % were considered for further analysis. Additionally, retention indices (RIs) were determined using a homologous series of n-alkanes (C_8-C_{20}) as standard references. The calculated RIs were then cross-referenced with those reported in the literature (16).

Assessment of antioxidant activity

2,2-diphenyl-1-picrylhydrazyl (DPPH) assay

The antioxidant activity of *C. amada* leaf essential oil was assessed using a previously described methodology with minor changes (17). Briefly, 1 mL of 0.01 mM DPPH solution was mixed with 1 mL of each prepared essential oil concentration (10-100 µg/mL) and the mixture was incubated at 37 °C for 30 min in the dark. The absorbance of the solution was measured at 517 nm using methanol as blank. The free radical scavenging potential of essential oil was expressed as percentage of inhibition, calculated using the following formula:

$$\% \text{ of inhibition} = (1 - OD_{sample} / OD_{control}) \times 100 \qquad \text{(Eqn. 1)}$$

2,2'-azino-bis (3-ethylbenzothiazoline-6-sulfonic acid (ABTS) assay

ABTS free-radical scavenging activity of the sample was assessed according to the protocol mentioned (17). An ABTS reagent was prepared by mixing 7 mM of ABTS solution with 2.45 mM of ammonium persulfate and then it was incubated for 16 hr at 37 ° C in dark. The ABTS solution was diluted with methanol, yielding an optical density (OD) of 0.70 ± 0.08 at 734 nm. Then, 0.3 mL of

various concentrations of the leaf oil (10-100 µg/mL) was mixed with 3 mL of the ABTS solution. This method was also carried out for ascorbic acid which was used as a positive control. The solution containing ABTS and methanol, excluding the sample was used as blank. The absorbance of the reaction mixture was measured using a UV-visible spectrophotometer at 734 nm. The inhibition (%) of ABTS free radicals was determined using the Eqn. 1 mentioned in the DPPH (2,2-diphenyl-1-picrylhydrazyl) assay.

Molecular docking analysis

In the present study, human Prdx5 (PDB ID: 1OC3), known for its antioxidant properties, was chosen for a molecular docking study. The three-dimensional crystal structures (".pdb" format) of the target protein was acquired from RCSB protein data bank (PDB) database (https://www.rcsb.org/). Subsequently, water molecules and heteroatoms, were removed from the receptor molecule. Additionally, polar H atoms were added to the target protein using BIOVIA Discovery Studio Visualizer 2019. Further, the model was adjusted for each side chain in the complex using SPDBv viewer through the "quick and dirty fixing" option (18). The final optimized protein structure was then saved in .pdb format. In the present study, a total of ten major phytoconstituents from *C. amada* having an area percentage greater than 2.50 % were chosen as potential antioxidant molecules (ligands).

The 3D conformers of these selected ligands, along with a standard compound (ascorbic acid), were obtained in a structured data format (SDF) from the NCBI-PubChem database (https://pubchem.ncbi.nlm.nih.gov/). Then, the SDF files were converted to PDB files using the BIOVIA Discovery Visualizer. Subsequently, the energies of all the chosen ligands were minimized using PyRx software. Molecular docking was conducted to assess the probable orientation and configuration of the ligands inside the binding site of the target protein. The 3D model (PDB format) of the receptor protein was imported into PyRx software. Next, a PDBQT file was generated that consisted of the protein structure with hydrogen atoms added to all polar residues.

The ligands were imported into PyRx software through the Open Babel plug-in tool, with subsequent energy minimization. All ligand bonds were set as rotatable to allow conformational flexibility. The docking point on the protein was established by adjusting the grid box around the binding site cavity at the following centres: X = 10.1645, Y = 6.1887 and Z = 39.1079. Further, to validate the docking protocol, it was initially removed from its respective receptors. Then, the ligand was re-docked into the same binding sites without applying any energy minimization steps. Final RMSD values were calculated by comparing the poses of the top-scored compounds with the initial pose of the co-crystallized ligand. For each ligand structure, ten runs were performed using AutoDock Vina and the best pose from each run was saved (19). Detailed visualization and comparison of the binding patterns of docked complexes, including bond lengths and types of interactions formed between ligands and proteins, were carried out using the BIOVIA Discovery Studio Visualizer.

Molecular dynamic simulation

The top screened compounds with the highest binding score were chosen for molecular dynamic simulation evaluations. The simulation module developed by SiBioLead LLC utilized GROMACS to evaluate the conformational changes in the protein -ligand complexes in comparison to the unbound apo-protein. The complexes were pre-processed with the optimized potentials for liquid simulations/all-atom (OPLS/AA) force field prior to simulation. The complexes were then placed in a triclinic periodic boundary box filled with a simple point charge water solvation model and a 0.15 M NaCl (sodium chloride) solution to maintain the counter ions concentration. This was followed by energy minimization using the steepest descent algorithm. Subsequently, NVT/NPT equilibration steps were performed over 100 ps each to stabilize the systems, maintaining a pressure of 1 bar and a temperature of 300 K. The simulated trajectories were analysed with the GROMACS analysis tool to measure various parameters, including RMSD, RMSF, radius of gyration (Rg), solvent accessible surface area (SASA), secondary structure analysis (DSSP), H-bond plots and binding-free energies (MM/PBSA).

Drug likeness and ADME/T prediction

SwissADME server (http://www.swissadme.ch/) and pkCSM online web tool (http://biosig.unimelb.edu.au/pkCSM/prediction) were used to predict physicochemical characteristics, drug likeness and medicinal chemical characteristics of the chosen compounds.

Density functional theory analysis

Quantum chemical methods were used to evaluate the electronic properties, potential reactivity and stability of the compounds. The molecular geometries of the studied compounds were optimized through density functional theory (DFT), employing B3LYP method with Becke's three-parameter exchange functional and the Lee-Yang-Parr nonlocal correlation functional using Avogadro and Gaussian 09 W software. B3LYP, a hybrid functional is useful for predicting frontier molecular orbitals, reactivity descriptors and non -covalent interactions. Furthermore, the computational analysis was performed using the 6-31G (d) basis set for each atom. The 6-31G (d) basis set includes polarization functions on heavy atoms, which improves the accuracy of electron density distribution-particularly important when evaluating properties such as HOMO-LUMO energies, MEP surfaces, ELF/LOL topologies and non-covalent interaction (NCI-RDG) analysis. This level of theory is well-suited for ground-state calculations and has been shown in prior literature to provide reliable insights for similar antioxidant and phytochemical systems (flavonoids, terpenes and essential oil components) (20-22). The equations used to determine the HOMO-LUMO energy gap and chemical reactivity parameters are outlined as follows:

Electronic affinity (A) = $- E_{LUMO}$ (Eqn. 2)

Ionization energy (I) = $- E_{HOMO}$ (Eqn. 3)

Electronegativity (X) = $- (E_{HOMO} + E_{LUMO})/2$ (Eqn. 4)

Chemical hardness (η) = $(E_{LUMO} - E_{HOMO})/2$ (Eqn. 5)

Chemical potential (µ) = $- \chi = (E_{HOMO} + E_{LUMO})/2$ (Eqn. 6)

Molecular softness (S) = $1/\eta$ (Eqn. 7)

Electrophilicity index (ω) = $\mu^2/2\eta$ (Eqn. 8)

Moreover, the topological parameters, including the noncovalent interactions (NCIs)-reduced density gradient (RDG) analysis, ELF and LOL analysis along with MEP maps were calculated using the atomistica online web server (https://atomistica.online/) (23), Multiwfn 3.7 Win 64 software (24) and VMD program (25), respectively.

Statistical analysis

The experimental data of the study were presented as mean ± SD (n = 3). Statistical analysis of the antioxidant assays was carried out using analysis of variance (ANOVA) followed by Tukey's multiple range test with *p* value less than 0.05 deemed significant. Analyses were performed using GraphPad Prism software (version 8.0; GraphPad, Sandiego, CA, USA).

Results and Discussion

Phytochemical profiling of CALEO

The essential oil extracted from *C. amada* was found to be pale yellow in colour, with an average yield of 0.35 % (v/w) determined on a fresh weight basis. However, a prior study reported 0.15 % (v/w) extraction yield from fresh leaves of *C. amada* collected from Northern India (26). The variations in the essential oil yield might be due to several factors such as geographical locations, difference in genotypes, environmental conditions and seasons during which samples were collected (27). GC-MS analysis of essential oil revealed 36 constituents, representing 90.03 % of the total leaf oil composition. In the current study, the leaf essential oil of *C. amada* was found to be rich in sesquiterpene alcohols (21.41 %) and monoterpene hydrocarbons (18.52 %) as represented in Table 1.

Table 1. Chemical constituents identified in the leaf essential oil of *Curcuma amada.*

S. No.	Compounds name	RI[a]	RI[b]	Peak area %	Identification[c]
1	Tricyclene	929	926	2.96 ± 0.08	RI, MS
2	α-pinene	947	939	4.68 ± 0.14	RI, MS
3	Camphene	977	954	7.23 ± 0.21	RI, MS
4	β-pinene	983	979	0.22 ± 0.01	RI, MS
5	p-cymene	1019	1024	0.31 ± 0.05	RI, MS
6	Limonene	1025	1029	1.56 ± 0.04	RI, MS
7	1,8-cineole	1028	1031	0.62 ± 0.03	RI, MS
8	Terpinolene	1101	1088	1.57 ± 0.19	RI, MS
9	Camphor	1153	1146	17.51 ± 0.52	RI, MS, STD
10	Camphene hydrate	1156	1149	0.95 ± 0.04	RI, MS
11	Isoborneol	1172	1160	2.07 ± 0.05	RI, MS
12	Terpinen-4-ol	1178	1177	0.49 ± 0.03	RI, MS
13	α-terpineol	1192	1188	0.59 ± 0.04	RI, MS
14	Myrtenol	1194	1195	0.92 ± 0.02	RI, MS
15	Myrtenyl acetate	1317	1326	0.22 ± 0.01	RI, MS
16	β-bourbonene	1376	1388	0.61 ± 0.03	RI, MS
17	β-elemene	1384	1390	2.79 ± 0.08	RI, MS
18	β-caryophyllene	1412	1419	2.68 ± 0.07	RI, MS
19	(Z)-β-farnesene	1445	1442	0.54 ± 0.02	RI, MS
20	allo-aromadendrene	1479	1460	0.45 ± 0.01	RI, MS
21	Curzerene	1486	1499	0.36 ± 0.01	RI, MS
22	δ-cadinene	1542	1523	0.43± 0.01	RI, MS
23	Germacrene B	1561	1561	0.47± 0.01	RI, MS
24	Spathulenol	1582	1578	12.00 ± 0.36	RI, MS
25	Ledol	1588	1602	0.91 ± 0.02	RI, MS
26	5-epi-7-epi-α-eudesmol	1602	1607	1.32 ± 0.03	RI, MS
27	γ-eudesmol	1614	1632	2.30 ± 0.06	RI, MS
28	epi-α-cadinol	1620	1640	0.45 ± 0.02	RI, MS
29	epi-α-muurolol	1625	1642	1.65 ± 0.05	RI, MS
30	β-eudesmol	1633	1650	0.82 ± 0.04	RI, MS
31	α-eudesmol	1642	1653	0.52 ± 0.02	RI, MS
32	α-cadinol	1653	1654	1.44 ± 0.05	RI, MS
33	ar-turmerone	1671	1669	4.60 ± 0.13	RI, MS
34	Germacrone	1686	1693	2.99 ± 0.08	RI, MS
35	Curdione	1715	1724	10.27 ± 0.30	RI, MS
36	14-hydroxy-α-muurolene	1761	1780	0.55 ± 0.02	RI
	Monoterpene hydrocarbon			18.52 ± 0.55	
	Sesquiterpene hydrocarbon			8.87 ± 0.26	
	Sesquiterpene alcohol			21.41 ± 0.64	
	Monoterpene alcohol			5.02 ± 0.15	
	Monoterpene ether			0.62 ± 0.01	
	Monoterpene ketone			17.51 ± 0.52	
	Monoterpene ester			0.22 ± 0.01	
	Sesquiterpene ketone			17.86 ± 0.53	
	Total identified			90.03 ± 2.70	

Data are represented as mean ± SD (n = 3). Compounds are listed in order of elution on the Elite-5 MS column. [a]Retention indices (**RI**) calculated against homologous n-alkane series (C8 - C20) on the Elite-5 MS column. [b]RI from literature (Adams 2007). [c]Identification methods: **MS**, comparison of mass spectra with NIST library; **RI**, comparison of retention index with those reported in literature; **STD**, comparison of mass spectra and retention time by authentic standard.

Camphor (17.51 %), spathulenol (12.00 %), curdione (10.27 %), camphene (7.23 %), α-pinene (4.68 %), ar-turmerone (4.60 %), germacrone (2.99 %), tricyclene (2.96 %), β-elemene (2.79 %) and β-caryophyllene (2.68 %) were the major compounds found in the leaf essential oil of *C. amada* as displayed in Fig. 1. Furthermore, γ-eudesmol (2.30 %), isoborneol (2.07 %), epi-α-muurolol (1.65 %), terpinolene (1.57 %), limonene (1.56 %), α-cadinol (1.44 %) and 5-epi-7-epi-α-eudesmol (1.32 %) were among the other compounds identified with peak area >1 %.

In comparison with other *Curcuma* species, a prior study reported that camphor was the predominant compounds followed by 1,8-cineole and isoborneol in the rhizome essential oil of *C. haritha* collected from southern India (28). However, camphor was found to be the predominant constituent in the leaf essential oil of *C. aromatica* collected from Kerala (29).

In-vitro antioxidant activity

The antioxidant potential of CALEO was evaluated by two distinct *in-vitro* colorimetric assays such as DPPH and ABTS assays, with ascorbic acid taken as reference antioxidant compound. The results revealed a dose-dependent increase in the free-radical scavenging activity with increasing CALEO concentrations (Table 2). CALEO exhibited significantly higher DPPH radical scavenging activity (IC_{50}= 6.91 ± 0.04 µg/mL compared to the positive control ascorbic acid (IC_{50}= 7.49 ± 0.06 µg/mL), with a significance level of $p < 0.001$. Similarly, the ABTS assay demonstrated slightly lower antiradical capabilities of CALEO with an IC_{50} value of 5.86 ± 0.06 µg/mL compared to ascorbic acid (IC_{50} = 4.33 ± 0.08 µg/mL) ($p < 0.001$) (Table 2). CALEO was found to be rich in terpenoids, which are well known for their potent antioxidant properties (30). Furthermore, previous studies on *Curcuma* species have also shown significant antioxidant effects, further supporting our findings (17, 31).

Molecular docking studies

Molecular docking was used to measure the binding interaction of the major constituents found in CALEO against the antioxidant Prdx5 protein (1OC3). A strong interaction between the molecule and the target protein is indicated by a more negative binding energy. The docking scores, amino acid residues involved and the nature of the interactions between the top 10 docked phytocompounds and the native ligand of the Prdx5 protein are summarized in Table 3. The binding energies of the respective configurations of the compounds docked with Prdx5 varied from -5 to -5.9 kcal/mol. Ascorbic acid with a docking score of -5.3 kcal/mol, primarily formed two conventional hydrogen bonds with the Cys47 and Arg127 residues at distances of 2.31 and 2.36 Å, respectively. Moreover, it also formed two carbons-hydrogen interactions with the Gly46 residue at a distance of 2.99 Å within the binding site of the Prdx5 protein.

However, β-caryophyllene (-5.9 kcal/mol), germacrone (-5.9 kcal/mol) and ar-turmerone (-5.8 kcal/mol) showed greater binding energies than the reference ligands. The optimal pose of β-caryophyllene had hydrophobic (alkyl) contact with the Pro45 residue of Prdx5 at a distance of 5.21 Å, while no further interactions were observed for the complex. β-caryophyllene showed substantial hydrophobic interactions but fewer H-bonds, indicating a more allosteric mode of stabilization. The ar-turmerone-Prdx5 complex exhibited good binding energy and was likely to bind to the binding pocket of Prdx5 by forming H-bonds with Arg127 (conventional) at a distance of 2.4 Å, π-alkyl interactions with Leu149 at a distance of 5.36 Å and alkyl bonds with the Leu116, Ile119 and Phe120 amino acid residues of Prdx5 at distances of 4.85, 5.37 and 4.71 Å, respectively.

Table 2. Antioxidant (DPPH and ABTS assay) activity of ascorbic acid and *Curcuma amada* leaf essential oil.

Sample/ standard	IC_{50} value	
	Antioxidant activity (µg/mL)	
	DPPH assay	ABTS assay
Essential oil	6.91±0.04	5.86± 0.06
Ascorbic acid	7.49± 0.06	4.33± 0.08

Positive control for DPPH and ABTS assay: ascorbic acid; statistical significance was measured by one-way analysis of variance followed by Tukey test. $^{ns}p > 0.05$, * $p < 0.05$ and ** $p < 0.01$ between the control and *C. amada* leaf essential oil for both DPPH and ABTS assays.

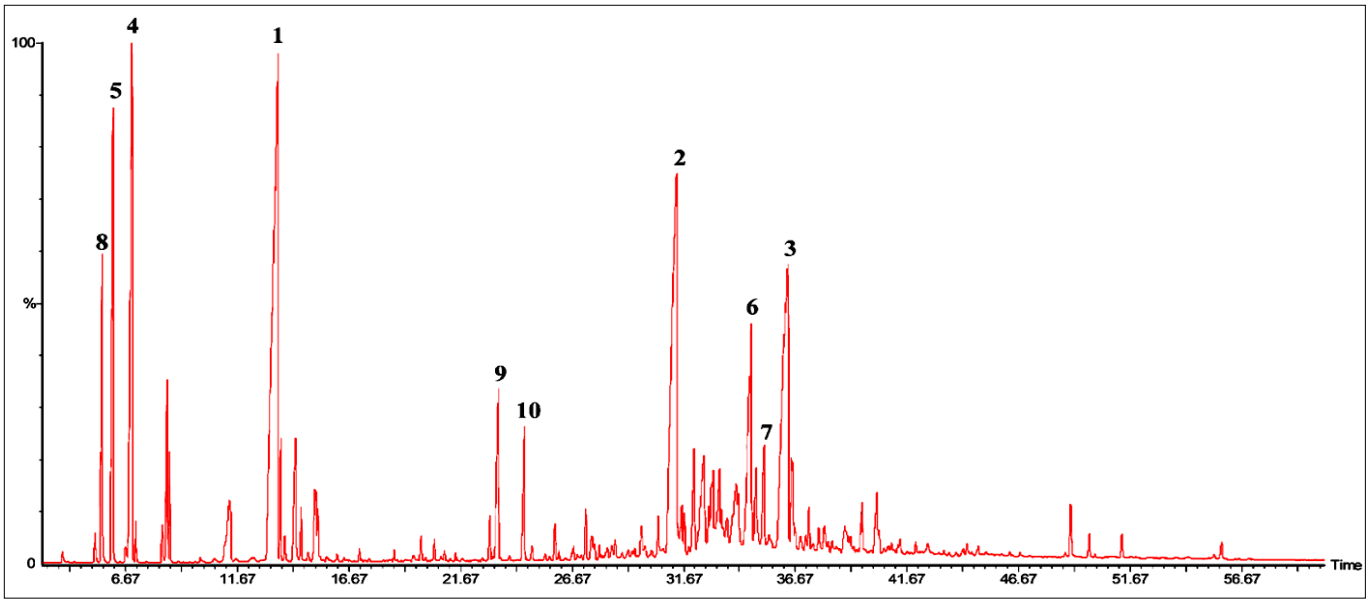

Fig. 1. GC-MS total ion chromatogram of the leaf essential oil of *Curcuma amada*. The numerical values given on the chromatogram represent the following compounds (**1**) camphor, (**2**) spathulenol, (**3**) curdione, (**4**) camphene, (**5**) α-pinene, (**6**) ar-turmerone, (**7**) germacrone, (**8**) tricyclene, (**9**) β-elemene and (**10**) β-caryophyllene.

Table 3. Binding affinities between major constituents derived from leaf essential oil of *C. amada* and the human target protein pero- xiredoxin5.

Protein	Compounds/ standard	Binding energy (kcal/mol)	No. of H-bonds	H-bond distance (Å)	H-bond interacting residues	Other interacting residues
Prdx5 (PDB ID: 1OC3)	α-pinene	-5.2	0	-	-	Pro40, Ala64, Phe120, Ile119, Leu116
	ar-turmerone	-5.8	1	2.4	Arg127	Leu116, Ile119, Phe120, Leu149
	β-caryophyllene	-5.9	0	-	-	Pro45
	β-elemene	-5.3	0	-	-	Pro45, Leu116, Phe120
	Camphene	-5	0	-	-	Cys47, Pro45
	Camphor	-5.1	2	2.01, 2.49	Gly46, Cys47	-
	Curdione	-5.1	1	2.39	Arg127	Thr147, Lys65
	Germacrone	-5.9	1	1.8	Gly46	-
	Spathulenol	-5.1	1	2.37	Lys33	Pro45
	Tricyclene	-5	0	-	-	Pro40
	Ascorbic acid	-5.3	3	2.31, 2.36, 2.99	Cys47, Arg127, Gly46	-

Ascorbic acid was used as the reference ligand for 1OC3 protein.

The observed interactions support the compound role in maintaining the catalytic efficiency of the enzyme, indicating its potential to mimic or enhance endogenous antioxidant signalling by stabilizing the conformation of Prdx5 under conditions of redox imbalance. The Prdx5-germacrone complex showed a H-bond interaction specifically with the Gly46 residue of the target protein at 1.80 Å. The strong hydrogen bond with Gly46 suggests an influence on the enzyme's peroxidative center, potentially enhancing its ability to neutralize ROS**.** Thus, the key residues involved in establishing the contacts between the top hit ligand poses of *C. amada* and the binding site of Prdx5 were Arg127, Gly46 and Cys47. These residues contributed to H-bonding and hydrophobic interactions, which helped to maintain the stability of the ligand–receptor complex.

The 2D and 3D representations of the interactions between the target protein and the top hit docked compounds derived from *C. amada* along with the reference ascorbic acid are displayed in Fig. 2. In this study, the heavy atom RMSD between the co-crystallized ligand and its redocked pose was determined as 0.0997 Å (< 2 Å), supporting the precision and reliability of the docking process.

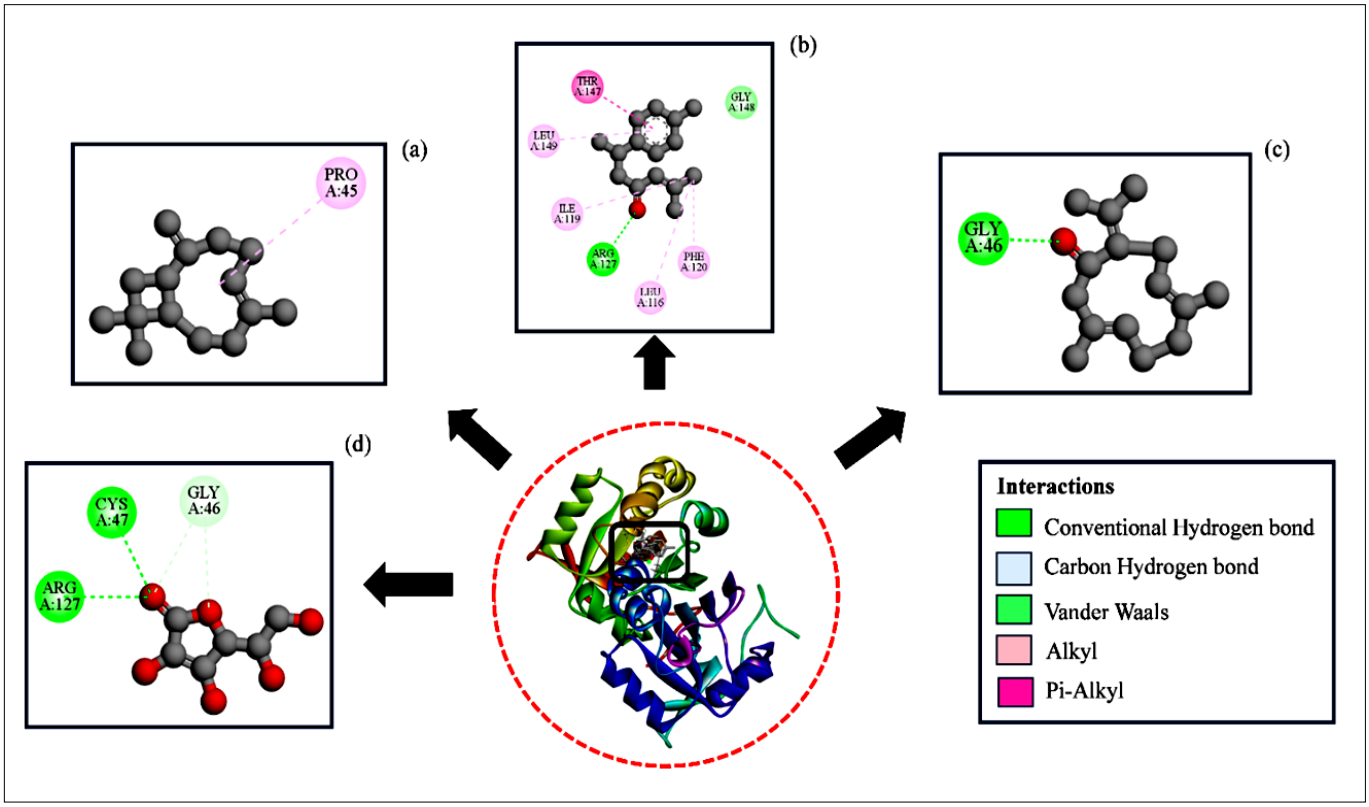

Fig. 2. Docked conformations of the top three bioactive phytocompounds obtained from *C. amada* leaf essential oil and the reference ligand (ascorbic acid) with target human-peroxiredoxin protein (PDB ID:1OC3). 2D visuals of (**a**) β-caryophyllene, (**b**) ar-turmerone, (**c**) germacrone and (**d**) standard (ascorbic acid) interacting with the binding site amino acid residues of Prdx5. The central 3D orientation in the circular closed region shows the overall binding site of the selected ligands and reference ligand within the target protein. The ligands are depicted in grey stick model; the hydrophobic and hydrogen bond acceptor/donor regions are annotated with interaction lines that are color-coded as per the legend (green: conventional hydrogen bond; light blue: carbon hydrogen bond; light green: van der Waals; light pink: alkyl and pink: pi-alkyl interactions.

MD simulation studies

RMSD the average distance between atoms of a protein structure over time, reflecting its flexibility (32). The RMSD score was calculated for each frame, with a higher RMSD indicating greater flexibility and a lower RMSD indicating better complex stability (Fig. 3a). The mean RMSD values for apo-Prdx5, Prdx5-β-caryophyllene, Prdx5-ar-turmerone, Prdx5-germacrone and Prdx5-ascorbic acid were 0.69 nm, 0.57 nm, 0.46 nm, 0.58 nm and 0.55 nm, respectively. The highest RMSD value was observed for apo-Prdx5, suggesting that the protein experiences conformational fluctuations in the absence of ligand interactions which may be due to the inherent flexibility or mobility of its constituent amino acids. However, Prdx5-β-caryophyllene, Prdx5-germacrone and the reference complex (Prdx5-ascorbic acid) showed nearly similar RMSD values with no statistically significant differences observed when compared to the apo-protein (adjusted p-value < 0.05), thereby, confirming the degree of rigidity of these complexes.

System variability may be indicated by minimal instability with lower RMSD values (33). In contrast, the average RMSD for the Prdx5-ar turmerone complex was the lowest over the 100 ns simulation (adjusted p-value < 0.05), indicating an optimal and stable binding mode between Prdx5 and ar-turmerone. Furthermore, the inherent flexibility of individual residues within the protein structure upon ligand binding was investigated using RMSF over the period of 100 ns simulation (Fig. 3b). The average RMSF changes for free Prdx5 and ligand-bound Prdx5 remained within the range of 0.2-0.3 nm, with standard deviation typically less than 0.05 nm across most residues, thereby, indicating that the binding of these ligands does not induce major conformational fluctuations in the amino acid residues of Prdx5.

In addition, ASP114, SER115, LEU116, VAL117, SER118, ILE119, PHE120, GLY121, GLN133, ASP134, GLY135, ILE136, VAL137 and LYS138 amino acid residues of the protein molecule were found to be actively involved in incorporating a high degree of fluctuations into apo-Prdx5. However, no such noticeable fluctuation was observed for ligated-Prdx5. The degree of structural compactness of the protein in the absence or presence of ligands was assessed by measuring the radius Rg. The mean Rg values for apo-Prdx5, Prdx5-β caryophyllene, Prdx5-ar turmerone, Prdx5-germacrone and Prdx5-ascorbic acid were determined to be 2.39 ± 0.03 nm, 2.33 ± 0.04 nm, 2.51 ± 0.08 nm, 2.36 ± 0.03 nm and 2.38 ± 0.03 nm, respectively.

Rg value that remains constant with minimal fluctuations throughout the MD simulation indicates a compact and folded protein structure, whereas significant variations in Rg over time may suggest structural instability or unfolding (34). The compactness of the Prdx5-β-caryophyllene and Prdx5-germacrone complexes was like those of apo-PRDX5 and the reference complex until the end of the simulation. However, the Prdx5-ar turmerone complex showed conformational fluctuations up to 66 ns, with a higher Rg value of 2.67 nm. This instability during the first half of the simulation could likely be a result of the initial binding phase of ar-turmerone, during which it might have undergone positional adjustments in flexible regions such as loops or terminal residues which require time to better align within the binding pocket of Prdx5. Subsequently, it followed a trajectory pattern similar to that of apo-Prdx5 after 80 ns (Fig. 3c).

Rg plots indicate that the protein-ligand complexes exhibit good stability with minimal alterations in protein compactness in the presence of ligands. SASA measures the surface area of a protein unit that may be available for interaction with the surrounding solvent molecules. The binding of a ligand to a protein may influence its structural characteristics, leading to changes in the SASA. A higher SASA value indicates reduced stability and structural expansion of the protein. The average SASA values for Prdx5-β caryophyllene (158.92 ± 2.41 nm^2), Prdx5-ar turmerone (160.27 ± 2.74 nm^2), Prdx5-germacrone (155.67 ± 2.59 nm^2) and Prdx5-ascorbic acid (159.56 ± 2.77 nm^2) were slightly greater than the SASA value of unbound Prdx5 (154.56 ± 2.80 nm^2). This finding suggests that the structure of Prdx5 slightly expanded upon contact with the ligands (Fig. 3d).

The formation of H-bonds between the protein and ligand stabilizes the complex (35). The conformational stability of the chosen complexes was further analysed by calculating the total number of hydrogen bonds formed between the protein and ligands across each frame during the 100 ns simulation (Fig. 3e). A greater number of H-bonds during the formation of protein –ligand complexes indicate a greater stability of the complex. The average numbers of intermolecular H-bonds formed in the Prdx5-ar turmerone (211), Prdx5-germacrone (210) and Prdx5-ascorbic acid (210) complexes were approximately the same as those in the nonligated protein Prdx5 (210), indicating the conformational stability of these complexes. However, the average number of intermolecular H-bonds formed between β-caryophyllene and Prdx5 (208) is slightly lower than that between β-caryophyllene and nonligated Prdx5. This finding suggested the reduced stability of the Prdx5-β-caryophyllene complex, may alter the native conformation of the protein.

Furthermore, variations in the secondary structure within the docked protein-ligand complexes were analysed to characterize the variability in the structural behaviour of the target protein bound to ligands in the binding site. The findings revealed that the conformational stability of apo- Prdx5 remained consistent throughout the simulation (Fig. 4). All the α-helices were maintained with occasional turns and bends in the initial primary residues, thus indicating the stability of the protein. The average secondary structure contents of the Prdx5-β-caryophyllene, Prdx5-ar-turmerone, Prdx5-germacrone and Prdx5-ascorbic acid complexes were relatively consistent with those of apo-Prdx5.

Binding free energy calculations using MM-PBSA

A final MD run was then conducted to acquire a more detailed understanding of the biomolecular interactions amongst the protein and ligand. The MM/PBSA analysis involved assessing the potential energy (electrostatic and van der Waals) and free solvation energy (polar and nonpolar) of each protein–ligand complex to calculate the total binding energy (ΔG) (Table 4). With the highest negative ΔG total value, the Prdx5-germacrone (-22.41 kcal/mol) complex exhibited the lowest energy state and the strongest binding affinity towards apo-Prdx5. The mean free binding energies for the Prdx5-β-caryophyllene, Prdx5-ar-turmerone and Prdx5-ascorbic acid complexes were estimated to be -20.44, -19.71 and -1.48 kcal/mol, respectively. Moreover, favourable van der Waals interactions between the protein and ligands are observed for

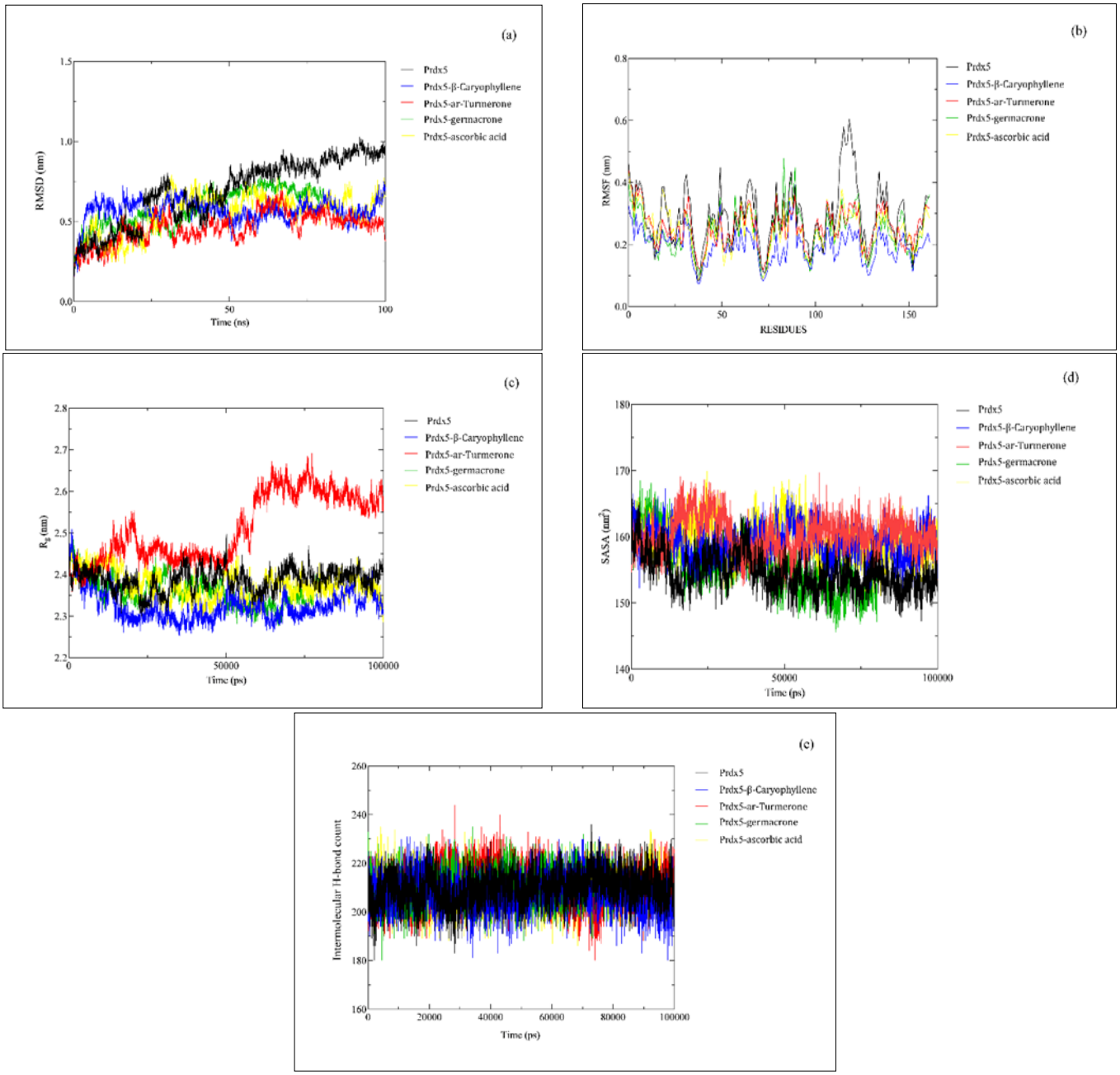

Fig. 3. MD simulation trajectories of apo-Prdx5 and selected protein-ligand docked complexes over the simulation period of 100 ns. (**a**) root mean square deviation of Cα atoms (RMSD), (**b**) root mean square fluctuation of Cα atoms (RMSF), (**c**) radius of gyration (Rg), (**d**) solvent accessible surface area (SASA) and (**e**) hydrogen bond formation of Prdx5 protein in ligand-bound and unbound conformation.

Table 4. MM-PBSA binding free energy analysis of the protein-ligand complexes.

Energy components (kcal/mol)	Prdx5-β-caryophyllene	Prdx5-ar-turmerone	Prdx5-germacrone	Prdx5-ascorbic acid
ΔVd Waals	-27.31	-26.73	-30.37	-2.58
ΔEEL	0.21	-1.84	-1.69	-0.36
ΔEPB	9.19	11.3	12.12	1.8
ΔENPOLAR	-2.52	-2.46	-2.47	-0.34
ΔG Gas	-27.1	-28.56	-32.06	-2.94
ΔG Solv	6.66	8.85	9.65	1.46
ΔG Total	-20.44	-19.71	-22.41	-1.48

Vd Waals: Vander Waals interactions, **EEL**: electrostatic energy, **EPB**: electrostatic polarization binding energy, **ENPOLAR**: non-polar solvation energy, **ΔG Gas**: Gibbs free energy in gas phase, **ΔG Solv**: solvation Gibbs free energy and **ΔG Total**: total Gibbs free energy.

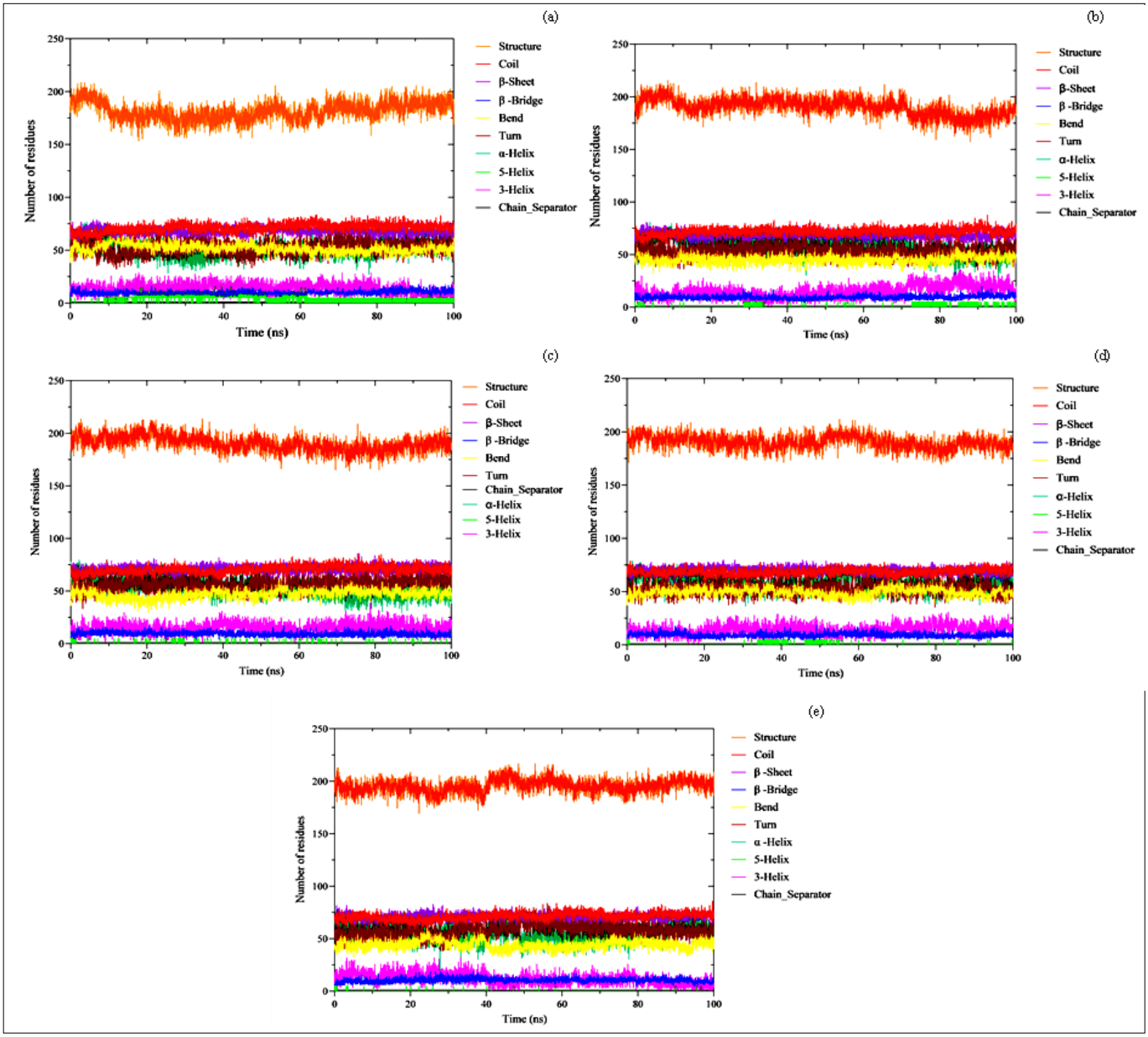

Fig. 4. Secondary structure changes while 100 ns simulation in (**a**) unbound-Prdx5, (**b**) β-caryophyllene-bound-Prdx5, (**c**) ar-turmerone bound-Prdx5, (**d**) germacrone bound-Prdx5 and (**e**) ascorbic acid bound-Prdx5 complexes.

all complexes, revealing a major contribution of nonspecific, short-range forces in stabilizing the complexes. Furthermore, the positive MM/PBSA results indicated the existence of unfavourable polar solvation contributing energies (EPB) for ligand binding. Upon ligand binding, this phenomenon is most likely due to the displacement of stabilizing water molecules surrounding the polar or charged groups, thereby, leading to increased solvation free energy (36).

ADME/T analysis

Pharmacological assessment

An absolute measure for drug discovery is the ability to estimate the fate and effects of the drug inside the body. Therefore, the drug likeness of the chosen compounds of CALEO was determined by applying a variety of filtering criteria, including Lipinski's rule of five (Ro5), Veber and Egan. In addition, the oral bioavailability of the selected chemical components was evaluated using the Abbott oral bioavailability score. Lipinski's rule of five states that a drug-like candidate must possess a molecular weight ≤ 500 Da, hydrogen bond donor (HBD) ≤ 5, hydrogen bond acceptor (HBA) ≤ 10, log $P_{o/w}$< 5, number of rotatable bonds ≤ 10 and topological polar surface area (TPSA) ≤ 140 Å^2.

The molecular weight threshold helps ensure that the chemical compound is adequately small to facilitate passage through the cell membrane. Drug absorption and distribution are facilitated by membrane permeability, which is primarily linked to the degree of lipophilicity of a drug candidate. The primary metric for quantifying lipophilicity in the octanol/water system is the partition coefficient P (*log p*). In addition, the interaction of a drug with proteins, membrane permeability, molecular affinity and solubility depend upon the presence of HBD and HBA in its structure. Lipinski's rule of five restricts the number of these donors and acceptors to maximize the capacity of the compound to participate in these interactions, avoiding excessive polarity or non-polarity, thereby improving its drug-likeness properties. The total number of rotatable bonds in a molecule is a significant component in determining its drug-like nature. A molecule must adopt a specific shape to bind to its target and cross cell membranes. If the molecule is originally stiff, it loses less entropy during the process. Therefore, a molecule must contain ≤ 10 rotatable bonds (37).

The topological polar surface area is another parameter representing the van der Waals surface area formed by polar atoms and reflects the H-bonding potential of any compound. It has been earlier reported that a polar surface area (PSA) of 20 to 140 Å^2 is ideal for drug absorption and distribution. Compounds with a PSA concentration outside this range are not suitable as drug candidates. Moreover, the Abbott oral bioavailability predicts the likelihood of a chemical compound having a score ≥ 10 % in rats. Previously stated, if a compound meets Lipinski's rule of five criteria, it typically achieves an Abbott bioavailability score of 0.55 (38). CALEO showed zero violations and adhered to Lipinski's rule of five. Consequently, high oral bioavailability (0.55) was also demonstrated for the compounds under study. In addition, Veber and Egan filters were applied to evaluate the drug likeness of the CALEO phytocompounds. The Veber filter restricts the number of rotatable bonds to ≤ 10 and the PSA to 140 Å^2. This restriction results from the unfavourable effects of the rotatable bond count and increased PSA on the drug permeation rate. Furthermore, Egan's rule specifies that compounds should have a TPSA ≤ 131.6 and a WLOGP ≤ 5.88. In the present study, all the chosen compounds met these criteria (Table 5).

Pharmacokinetic and toxicity assessment

An essential characteristic of oral medications is their solubility in intestinal fluid, as inadequate solubility may restrict intestinal absorption through the portal vein. Thus, drugs designed for intravenous delivery must be highly soluble in water to provide enough of the active component. Supplementary Table S1 shows the varying solubilities of the compounds from *C. amada*. CALEO compounds have a distribution of Silicos-IT LogSw values between -10 and 0, which corresponds to the acceptable range of values. Caco-2 (human colorectal adenocarcinoma epithelial) cells are often used as an experimental model to mimic the intestinal mucosa of humans to anticipate the degree to which drugs taken orally can be absorbed. Caco-2 permeability values (*log* Papp > 8 × 10^{-6}) results in a projected value > 0.90, signifying high Caco-2 permeability and ease of absorption of the compounds.

Among the studied compounds, ar-turmerone was predicted to have high Caco-2 permeability, indicating a high likelihood of reaching systemic circulation. The intestine is recognised as the primary location where drugs are absorbed following oral administration. Intestinal absorption (IA) measures the percentage of a drug absorbed through the human intestine. A greater gastrointestinal (GI) absorption score suggests an increased likelihood that a chemical compound will be transported to various tissues in the body through the circulatory system. An absorbance rate less than 30 % suggests poor intestinal absorption in humans. However, β-caryophyllene, ar-turmerone and germacrone showed very high intestinal absorption rates (> 90 %). Skin permeation refers to the capacity of a molecule to permeate through skin tissue. It determines whether a substance is likely to be skin permeable and is stated in terms of the skin permeability constant, logKp (cm/h). A logKp value greater than -2.5 indicates that a compound has relatively poor skin permeability. These findings imply that β-caryophyllene and ar-turmerone have moderate skin permeability.

CNS is protected by ATP-binding cassette transporters (ABC transporters), among which P-gp has been found to be the primary building component. Drugs have been reported to be transported across biological membranes through ABC transporters. No P-gp substrate or inhibitor was detected in any of the investigated phytocompounds. Furthermore, four potential parameters, namely, the volume of distribution (VDss), fraction unbound (human), blood-brain barrier membrane permeability (BBB) and CNS permeability, were taken into consideration while analysing their dispersion. The distribution of drugs in different *in vivo* tissues is described by the volume of distribution (VDss). A VDss of less than 0.71 L kg^{-1} (log VDss < -0.15) indicates a limited volume of distribution. Moreover, a VDss greater than 2.81 L kg^{-1}(log VDss > 0.45) indicates a substantially large distribution volume.

Among the tested compounds, β-caryophyllene had the highest VDss. Moreover, the drug-associated side effects and toxicities may be prevented through monitoring the capacity of a drug to cross the blood-brain barrier (BBB). The BBB value of an ideal drug should range between -3.0 and 1.2. β-Caryophyllene had the greatest effect on BBB permeability, followed by germacrone and ar-turmerone (*log* BB > 0.3). The blood-brain permeability surface area product or central nervous system (CNS) permeability indicates a logarithmic relationship between the concentration of drugs in the brain and that in the blood. These compounds have limited CNS permeability, suggesting that while they may cross the BBB, their penetration into the CNS may not be sufficient for significant neurological effects.

The metabolism of the compounds was evaluated based on whether they are inhibitors or substrates of cytochrome P450 (CYPP450) isozymes. CYPP450 is a detoxifying enzyme in the liver that oxidizes xenobiotics and facilitates their excretion. Since CYPP450 isoforms may destroy or activate numerous drugs, it is critical to evaluate the capacity of compounds to inhibit CYPP450. None of the compounds, including β-caryophyllene, ar-turmerone, germacrone, or ascorbic acid, act as substrates for major CYP450 enzymes, such as CYP2D6 and CYP3A4, showing minimal participation in these crucial metabolic pathways. However, ar-turmerone acts as a CYP1A2 inhibitor, establishing its ability to control the activity of this enzyme, thereby

Table 5. Drug-likeliness and physicochemical properties of selected compounds.

Compounds	Molecular weight (g/mol)	No. of H-bond donors	No. of H-bond acceptors	No. of rotatable bonds	TPSA (Å^2)	MLOGP	WLOGP	Lipinski rules	Veber rules	Egan rules	Abbott bioavailability score
ar-turmerone	216.32	0	1	4	17.07	3.68	4.02	yes	yes	yes	0.55
Germacrone	218.33	0	1	0	17.07	3.37	4.36	yes	yes	yes	0.55
β-caryophyllene	204.35	0	0	0	0.00	4.63	4.73	yes	yes	yes	0.55
Ascorbic acid	176.12	4	6	6	107.22	-2.6	-1.41	yes	yes	yes	0.56

TPSA: topological polar surface area, **MLOGP**: moriguchi-octanol water partition coefficient and **WLOGP**: water partition coefficient.

influencing the metabolism of other drugs that act through CYP1A-mediated pathways. Moreover, none of the compounds inhibited other CYP enzymes, such as CYP2D6, CYP2C9, CYP3A4 or CYP2C19, which reduces the risk of potential drug interactions through these pathways.

Total drug clearance (CLtot) is a factor influenced by the combination of hepatic and renal clearance, which has a substantial impact on bioavailability, dosage rates and half-life. In addition, the hydrophilicity and molecular weight of substances affect drug clearance. The prediction results suggested that germacrone exhibits more efficient clearance from the body than other compounds. Renal uptake transporters include organic cation transporter 2 (OCT2). During the first stage of the elimination process, molecules are drawn from the blood into renal tubular cells, where they play a crucial role in the renal clearance of ionized drugs and endogenous components (39). None of the chosen CALEO compounds were anticipated to be substrates for OCT2.

Among the main causes of drug discovery failure in its latter stages is the amount of harm that any compound may cause to the organs of the organism. Therefore, early toxicity monitoring would be very useful. Few toxicity-related factors were determined for CALEO compounds using the pkCSM pharmacokinetics online tool. The AMES test is a bacterial-based mutagenicity assay that is used to determine the mutagenic potential of any compound. A positive result implies that the substance is mutagenic, which may lead to the emergence of cancer. The AMES test revealed no toxicity for any of the CALEO compounds. The human ether-a-go-go-related gene (*hERG*) encodes a potassium ion (K^+) channel that is associated with prolonged ventricular repolarization periods and QT intervals. Each of these factors increases the risk of arrhythmia and heart failure. Therefore, accurate predictions of the cardiac toxicity of drugs in the initial phases of drug development are essential, as *hERG*/K^+ channel blockers could be hazardous. Interestingly, none of the CALEO compounds blocked the *hERG* I or *hERG* II channels, which indicated a low probability of cardiac arrhythmias. The biotransformation of xenobiotics and energy exchange depend primarily on the liver. Liver damage frequently impairs normal metabolism, which may lead to liver failure. The selected compounds of CALEO were not expected to be hepatotoxic (Supplementary Table S1).

DFT studies

The major components with the highest binding scores were presumed to be responsible for the antioxidant properties of CALEO. Thus, the chemical reactivity of these compounds was investigated further using DFT. Electron excitation and transmission at the molecular level are determined by the highest occupied molecular orbital (HOMO) and lowest occupied molecular orbital (LUMO) energies (40). A higher E_{HOMO} value indicates strong antioxidant or antiradical properties, with germacrone-demonstrating this characteristic (20). Moreover, FMO calculations estimate the energy difference between the HOMO and LUMO states, which can be used to predict the reactivity and stability of any molecule.

A smaller energy gap (Eg) in a molecule result in greater flexibility due to its high polarizability, low kinetic stability and strong chemical reactivity. However, a molecule with a larger Eg is regarded as stable and possesses a high chemical hardness (41). The resistivity of a molecule to cloud polarization or deformation is measured by its chemical hardness (η). Smaller η values suggest greater susceptibility to deformation and enhanced reactivity (42). According to the estimated Eg and η values, β-caryophyllene (3.239 eV) exhibited the highest predicted chemical hardness and ar-turmerone (2.430 eV) showed the lowest.

Thus, ar-turmerone is the most reactive antioxidant/antiradical in CALEO, even compared to ascorbic acid, in terms of susceptibility to deformation or reaction. The ionization potential (IP) is helpful for estimating reactivity because it indicates the ability of a compound to scavenge free radicals through an electron transfer process. A lower IP value suggests easier release of electrons, which increases the reactivity towards free radicals. A negative chemical potential (μ) represents electronegativity (χ), which indicates the ability of a molecule to draw electrons. A higher χ signifies greater attraction of electrons, leading to increased chemical reactivity. Thus, ar-turmerone, with the lowest IP and highest electronegativity, exhibits the highest reactivity in neutralizing free radicals by contributing a single electron. The obtained FMO plots and estimated global reactivity descriptor values for the studied compounds are summarized in Supplementary Table S2.

In the present study, MEP maps were plotted to analyse the distribution of nuclear and electronic charges in the areas surrounding a molecule and to predict the chemical reactivity, size, shape and sites of reactivity of the studied compounds against the reference compound ascorbic acid. The MEP plots of β-caryophyllene, germacrone, ar-turmerone and ascorbic acid showed an electrostatic potential (EP) range of -3×10^{-6} to 3×10^{-6} atomic units. Low-density (high potential) regions act as electrophilic centers, whereas high-density (low potential) regions act as nucleophilic centers (43). These nucleophilic centers may indicate areas susceptible to electron donation, whereas electrophilic centers may indicate regions prone to electron acceptance.

The MEP values decreased in the following order: blue > green > yellow > orange > red. The blue region depicts the maximum nucleophilic reactivity and the red region depicts the maximum electrophilic reactivity. The green region corresponds to zero EP, whereas intermediate potential regions, depicted in yellow and orange, lie between the neutral (zero) and electrophilic (red) regions (44). The MEP plots of the studied compounds are displayed in Fig. 5 (left -a, b, c and d).

The radical scavenging properties of biomolecules primarily depend on their ability to transfer charges easily, which is determined by the nature of the bond developed between them. Topological analysis, such as ELF and LOL analysis, were conducted to understand the characteristics of these bonds. The chemical properties of ELF and LOL are comparable since they both rely on the kinetic energy density (45). The ELF map ranges between 0 and 1, where regions < 0.5 suggest delocalized electrons, while LOL shows high values (> 0.5) in the areas where electron localization is prominent (46). Fig. 5 (right -a, b, c and d) illustrates the ELF and LOL contour maps. Red areas indicate high ELF values around the central atom, which could be caused by a nuclear layer or covalent bond. However, blue zones represent electron-depleted

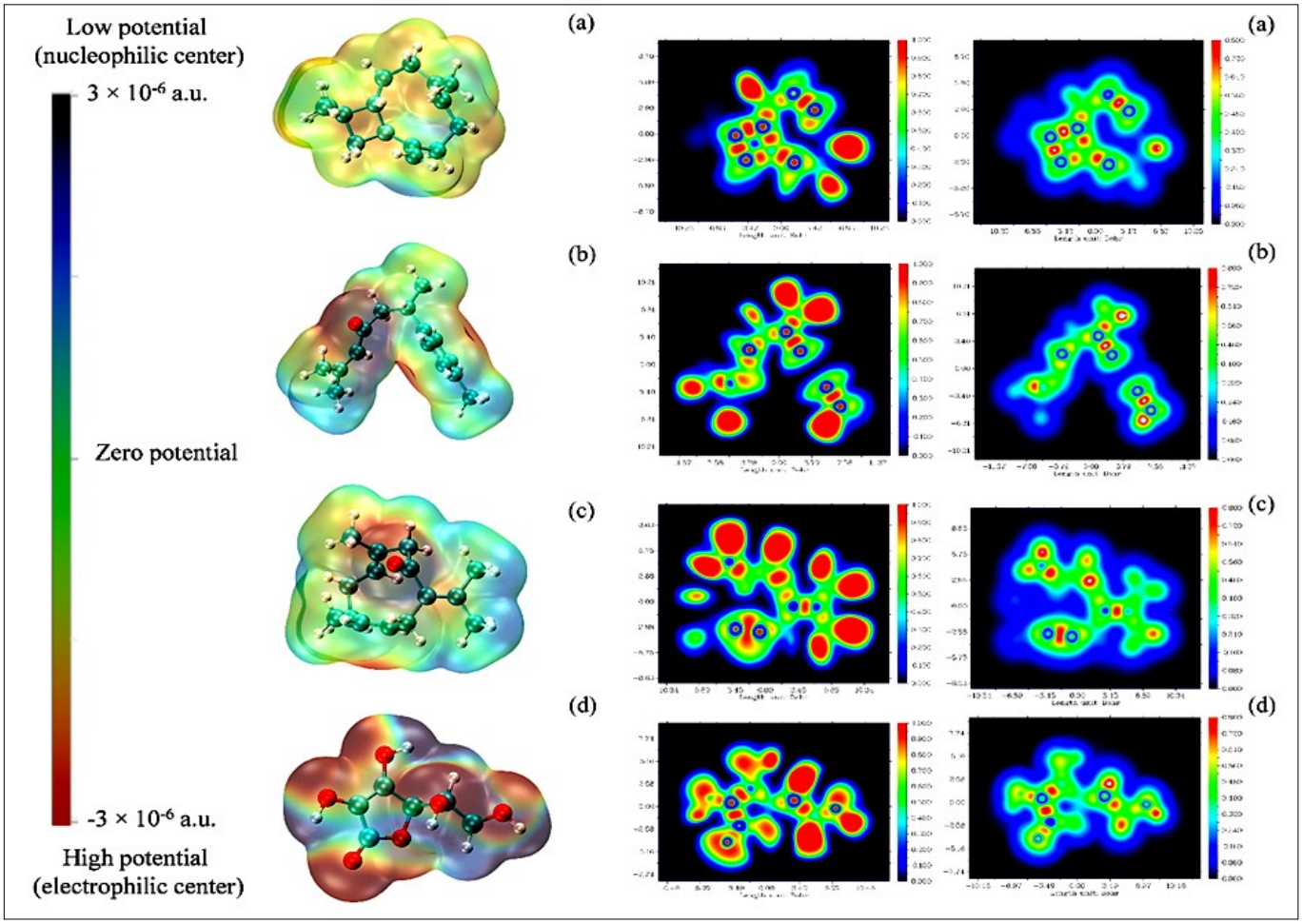

Fig. 5. Molecular electrostatic potential (MEP) surface maps (left) and ELF/LOL color filled maps (right) of the DFT optimized structures. (**a**) β-caryophyllene, (**b**) ar-turmerone, (**c**) germacrone and (**d**) ascorbic acid (standard). The vertical color scale adjacent to the MEP map ranges from blue (low potential, nucleophilic region) tored (high potential, electrophilic region). ELF and LOL maps use a similar color gradient, where red indicates high and blue indicates low electron localization, respectively.

regions for all the studied compounds. In the LOL contour maps, the outer white shell appeared white in the central areas of the compounds under study, indicating that the electron density exceeded the highest point of the colour scale bar (0.8).

Molecular interactions play a key role in determining the stability of a molecular structure. These interactions are identified through reduced density gradient (RDG) analysis, which specifically targets the noncovalent interactions (NCIs) within the system. NCI plots allowed visualization of strong directional attractions associated with localized atom–atom contacts and regions of weak interactions (47). The NCI-RDG gradient iso surfaces and 2D plots of the studied compounds are displayed in Fig. 6. The spikes or peaks observed in the 2D scatter plots correspond to interaction critical points (ICPs).

The electron density within the ICP range determines the strength of a noncovalent interaction. The electron density values below zero ($\lambda_2 < 0$) (blue-coloured iso surface), above zero ($\lambda_2 > 0$) (red-coloured iso surface) and spikes with a value nearly zero ($\lambda_2 \approx 0$) at the ICP represent stronger attractions, repulsive interactions and presence of weak van der Waals interactions, respectively. Thus, the findings of the current study revealed that the strongest steric repulsion was observed for ar-turmerone near the center of the aromatic ring, which may be due to π-π stacking interactions.

Conclusion

In the present study, the chemical composition, *in-vitro* and *in silico* antioxidant activities of *C. amada* leaf essential oil was evaluated to establish its potential health benefits. GC-MS analysis identified sesquiterpene alcohols (21.41 %) as the predominant group, with camphor (17.51 %) as the key constituent. CALEO exhibited significant antioxidant activity. Molecular docking analysis revealed that ar-turmerone, β-caryophyllene and germacrone possess high efficacy in mitigating oxidative stress by interacting with target protein residues. This was further confirmed through molecular docking (MD) simulations and MM/PBSA analysis. The core constituents with strong binding scores were subsequently subjected to frontier molecular orbital (FMO) analysis, which, in combination with conceptual density functional theory (DFT) calculations, further confirmed the antioxidant potential of the studied compounds. Additionally, ADMET profiling indicated drug-likeness, good bioavailability and favourable safety profiles of these compounds. Although Prdx5 is not a direct Nrf2 target, its stabilization by CALEO compounds may indirectly support redox homeostasis and attenuate oxidative stress-induced NF-κB signaling. Overall, this study highlights CALEO phytocompounds as promising and safer alternatives to synthetic drugs for managing oxidative stress. However, further *in-vivo* studies are necessary to validate the therapeutic efficacy and safety of these compounds for oxidative stress-related disorders.

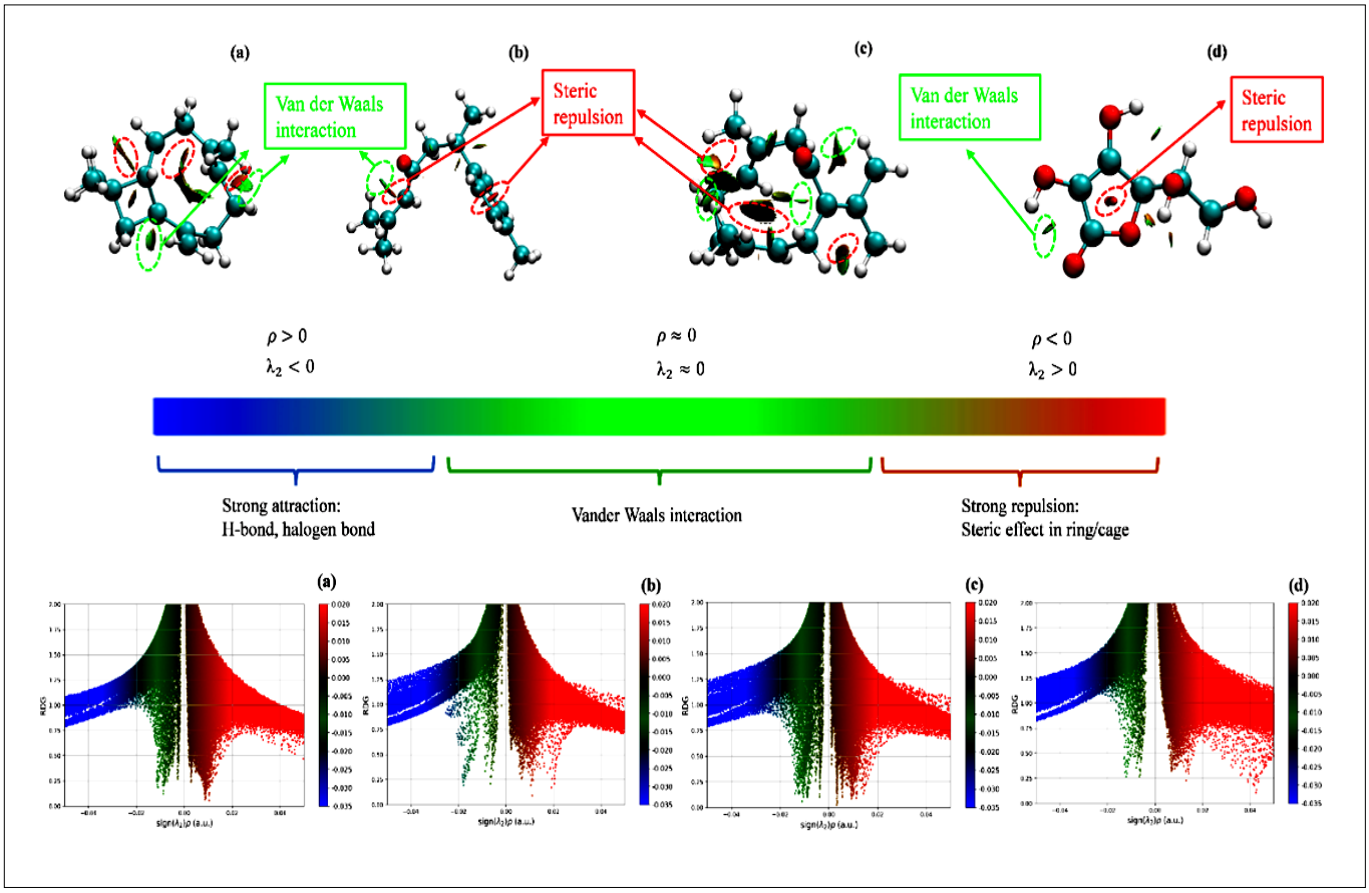

Fig. 6. 2D colored scatter plot and RDG iso surface density plot (**a**) β-caryophyllene (**b**) ar-turmerone (**c**) germacrone and (**d**) ascorbic acid (standard).

Acknowledgements

The authors are grateful to Dr. Debajyoti Das, Dean, Centre for Biotechnology and Dr. MR Nayak, President, Siksha 'O' Anusandhan (Deemed to be University) for providing facilities and encouragement.

Authors' contributions

AP conducted the research, analysed the data and wrote the manuscript. DM assisted with data analysis. AS, BD, PCP and SN reviewed and edited the manuscript. AR and SJ contributed to the initial concept, designed the study and investigated relevant areas. All authors read and approved the final manuscript.

Compliance with ethical standards

Conflict of interest: Authors do not have any conflict of interests to declare.

Ethical issues: None

References

1. Pisoschi AM, Pop A. The role of antioxidants in the chemistry of oxidative stress: A review. Eur J Med Chem. 2015;97:55-74. https://doi.org/10.1016/j.ejmech.2015.04.040
2. Adardour M, Ait Lahcen M, Oubahmane M, Ettahiri W, Hdoufane I, Bouamama H, et al. Design, synthesis, molecular modeling and biological evaluation of novel pyrazole benzimidazolone derivatives as potent antioxidants. Pharmaceuticals. 2023;16 (12):1648. https://doi.org/10.3390/ph16121648
3. Pizzino G, Irrera N, Cucinotta M, Pallio G, Mannino F, Arcoraci V, et al. Oxidative stress: Harms and benefits for human health. Oxid Med Cell Longev. 2017;2017:8416763. https://doi.org/10.1155/2017/8416763
4. Andrés Juan C, Pérez de Lastra JM, Plou Gasca FJ, Pérez-Lebeña E. The chemistry of reactive oxygen species (ROS) revisited: Outlining their role in biological macromolecules (DNA, lipids and proteins) and induced pathologies. Int J Mol Sci. 2021;22:4642. https://doi.org/10.3390/ijms22094642
5. Pham-Huy LA, He H, Pham-Huy C. Free radicals, antioxidants in disease and health. Int J Biomed Sci. 2008;4:89.
6. Deponte M. Glutathione catalysis and the reaction mechanisms of glutathione-dependent enzymes. Biochem Biophys Acta. 2013;1830:3217-66. https://doi.org/10.1016/j.bbagen.2012.09.018
7. Knoops B, Goemaere J, Van der Eecken V, Declercq JP. Peroxiredoxin 5: Structure, mechanism and function of the mammalian atypical 2-Cys peroxiredoxin. Antioxid Redox Sig. 2011;15(3):817-29. https://doi.org/10.1089/ars.2010.3584
8. Walbrecq G, Wang B, Becker S, Hannotiau A, Fransen M, Knoops B. Antioxidant cytoprotection by peroxisomal peroxiredoxin-5. Free Radic Biol Med. 2015;84:215-26. https://doi.org/10.1016/j.freeradbiomed.2015.02.032
9. Devcich DA, Pedersen IK, Petrie KJ. You eat what you are: Modern health worries and the acceptance of natural and synthetic additives in functional foods. Appetite. 2007;48 (3):333 -37. https://doi.org/10.1016/j.appet.2006.09.014
10. Chen Y, Shukurova MK, Asikin Y, Kusano M, Watanabe KN. Characterization of volatile organic compounds in mango ginger (*Curcuma amada* Roxb.) from Myanmar. Metabolites. 2020;11(1):21. https://doi.org/10.3390/metabo11010021
11. Choudhary L, Rasool MA, Pounikar Y, Ahirwar DK, Jain R, Sahu S. *In-silico* investigation of various phytoconstituents present in mango ginger (*Curcuma amada* Roxb.) as antibacterial agents.

Afr J Bio Sci. 2024;6(14):451-59. https://doi.org/10.48047/AFJBS.6.8.2024.450-459

12. Policegoudra RS, Aradhya SM, Singh L. Mango ginger (*Curcuma amada* Roxb.) - A promising spice for phytochemicals and biological activities. J Biosci. 2011;36(4):739–48. https://doi.org/10.1007/s12038-011-9106-1
13. Karmakar I, Dolai N, Saha P, Sarkar N, Bala A, Haldar PK. Scavenging activity of *Curcuma caesia* rhizome against reactive oxygen and nitrogen species. Orient Pharm Exp Med. 2011;11(4):221-28. https://doi.org/10.1007/s13596-011-0030-6
14. Hassan W, Gul S, Rehman S, Kanwal F, Afridi MS, Fazal H, et al. Gas chromatography coupled with mass spectrometric characterization of *Curcuma longa*: Protection against pathogenic microbes and lipid peroxidation in rat's tissue homogenate. Pak J Pharm Sci. 2016;29(2):615-21.
15. European Pharmacopoeia. European Pharmacopoeia Commission and European Directorate for the Quality of Medicines Healthcare 7th ed. 2010. Available from: https://www.edqm.eu/en/
16. Adams RP. Identification of essential oil components by gas chromatography/mass spectroscopy. 4th ed. Illinois (IL): Allured Publishing Corporation; 2007.
17. Jena S, Ray A, Banerjee A, Sahoo A, Nasim N, Sahoo S, et al. Chemical composition and antioxidant activity of essential oil from leaves and rhizomes of *Curcuma angustifolia* Roxb. Nat Prod Res. 2017;31(18):2188-91. https://doi.org/10.1080/14786419.2017.1278600
18. Guex N, Peitsch MC. SWISS-MODEL and the Swiss-Pdb Viewer: An environment for comparative protein modeling. Electrophoresis. 1997;18(15):2714-23. https://doi.org/10.1002/elps.1150181505
19. Herowati R, Widodo GP. Molecular docking studies of chemical constituents of *Tinospora cordifolia* on glycogen phosphorylase. Procedia Chem. 2014;13:63-68. https://doi.org/10.1016/j.proche.2014.12.007
20. Tasheh NS, Fouegue AD, Ghogomu JN. Investigation of the antioxidant and UV absorption properties of 2-(2'-hydroxy-5'-methylphenyl)-benzotriazole and its ortho-substituted derivatives via DFT/TD-DFT. Comput Chem. 2021;9(3):161-96. https://doi.org/10.4236/cc.2021.93010
21. Zochedh A, Priya M, Shunmuganarayanan A, Thandavarayan K, Sultan AB. Investigation on structural, spectroscopic, DFT, biological activity and molecular docking simulation of essential oil gamma-terpinene. J Mol Struct. 2022;1268:133651. https://doi.org/10.1016/j.molstruc.2022.133651
22. Acidi A, Siakhene N, Grine S, Bouasla R, Rizi A, Otmane Rachedi K, et al. *In vitro* and *in silico* studies of antifungal activity of *Syzygium aromaticum* essential oil and its main constituent 'eugenol' against a citrus fungal strain, *Fusarium proliferatum*. Chem Afr. 2025;8(4):1365-76. https://doi.org/10.1007/s42250-025-01225-z
23. Armaković S, Armaković SJ. Atomistica. Online-web application for generating input files for ORCA molecular modelling package made with the Anvil platform. Mol Simul. 2023;49(1):117-23. https://doi.org/10.1080/08927022.2022.2126865
24. Lu T, Chen F. Multiwfn: A multifunctional wavefunction analyzer. J Comput Chem. 2012;33(5):580-92. https://doi.org/10.1002/jcc.22885
25. Humphrey W, Dalke A, Schulten K. VMD: Visual molecular dynamics. J Mol Graph. 1996;14(1):33-38. https://doi.org/10.1016/0263-7855(96)00018-5
26. Padalia RC, Verma RS, Sundaresan V. Volatile terpenoid compositions of leaf and rhizome of *Curcuma amada* Roxb. from Northern India. J Essent Oil Res. 2013;25(1):17-22. https://doi.org/10.1080/10412905.2012.747271
27. Kumar S, Yadav M, Yadav A, Yadav JP. Impact of spatial and climatic conditions on phytochemical diversity and *in vitro* antioxidant activity of Indian *Aloe vera* (L.) Burm. f. South Afr J Bot. 2017;111:50–59. https://doi.org/10.1016/j.sajb.2017.03.012
28. Raj G, Baby S, Dan M. Volatile constituents from the rhizomes of *Curcuma haritha* Mangaly and Sabu from southern India. Flavour Fragr J. 2008;23(5):348-52. https://doi.org/10.1002/ffj.1891
29. Albaqami JJ, Hamdi H, Narayanankutty A, Visakh NU, Sasidharan A, Kuttithodi AM, et al. Chemical composition and biological activities of the leaf essential oils of *Curcuma longa*, *Curcuma aromatica* and *Curcuma angustifolia*. Antibiotics. 2022;11(11):1547. https://doi.org/10.3390/antibiotics11111547
30. Ray A, Jena S, Dash B, Kar B, Halder T, Chatterjee T, et al. Chemical diversity, antioxidant and antimicrobial activities of the essential oils from Indian populations of *Hedychium coronarium* Koen. Ind Crops Prod. 2018;112:353-62. https://doi.org/10.1016/j.indcrop.2017.12.033
31. Sahoo A, Jena S, Ray A, Dash KT, Nayak S, Panda PC. Chemical constituent analysis and antioxidant activity of leaf essential oil of *Curcuma xanthorrhiza*. J Essent Oil-Bear Plants. 2021;24(4):736-44. http://dx.doi.org/10.1080/0972060X.2021.1955750
32. Pundir H, Pant M, Joshi T, Bhat S, Pathak R, Bajpai AB, et al. Identification of essential oil phytocompounds as natural inhibitors of odorant-binding protein to prevent malaria through *in silico* approach. J Biomol Struct Dyn. 2023;41:8323-33. https://doi.org/10.1080/07391102.2022.2132419
33. Kuzmanic A, Zagrovic B. Determination of ensemble-average pairwise root mean-square deviation from experimental B-factors. Biophys J. 2010;98:861-71. https://doi.org/10.1016/j.bpj.2009.11.011
34. MIu L, Bogatyreva NS, Galzitskaia OV. Radius of gyration is indicator of compactness of protein structure. Mol Biol. 2008;42:701-706.
35. Panigrahi SK. Strong and weak hydrogen bonds in protein-ligand complexes of kinases: A comparative study. Amino Acids. 2008;34:617–33. https://doi.org/10.1007/s00726-007-0015-4
36. Maurer M, Oostenbrink C. Water in protein hydration and ligand recognition. J Mol Recog. 2019;32(12):e2810. https://doi.org/10.1002/jmr.2810
37. Schneckener S, Grimbs S, Hey J, Menz S, Osmers M, Schaper S, et al. Prediction of oral bioavailability in rats: Transferring insights from *in vitro* correlations to (deep) machine learning models using *in silico* model outputs and chemical structure parameters. J Chem Inf Model. 2019;59:4893-905. https://doi.org/10.1021/acs.jcim.9b00460
38. Martin YC. A bioavailability score. J Med Chem. 2005;48:3164-70. https://doi.org/10.1021/jm0492002
39. Belal A. Drug likeness, targets, molecular docking and ADMET studies for some indolizine derivatives. Pharmazie. 2018;73:635-42. https://doi.org/10.1691/ph.2018.8061
40. Ramírez-Martínez C, Zárate-Hernández LA, Camacho-Mendoza RL, González-Montiel S, Meneses-Viveros A, Cruz-Borbolla J. The use of global and local reactivity descriptors of conceptual DFT to describe toxicity of benzoic acid derivatives. Comput Theor Chem. 2023;1226:114211. https://doi.org/10.1016/j.comptc.2023.114211
41. Akman F. A density functional theory study based on monolignols: Molecular structure, homo-lumo analysis, molecular electrostatic potential. Cellul Chem Technol. 2019;53(3-4):243-50. http://dx.doi.org/10.35812/CelluloseChemTechnol.2019.53.24
42. Ngo TC, Dao DQ, Thong NM, Nam PC. Insight into the antioxidant properties of non-phenolic terpenoids contained in essential oils extracted from the buds of *Cleistocalyx operculatus*: A DFT study. RSC Adv. 2016;6:30824-34.

43. Khnifira M, Boumya W, Attarki J, Soufi A, Sadiq MH, Achak M, et al. Interaction between drug molecule and inverse spinel surfaces in aqueous solution: Insights from DFT and DMC simulation. Comput Theor Chem. 2023;1228(9):114289. https://doi.org/10.1016/j.comptc.2023.114289

44. Grine S, Taibi F, Berredjem M, Dekir A, Benaliouche F, Rachedi KO. Antifungal activity of the essential oil of *Pelargonium graveolens*. Molecular docking, molecular dynamics, DFT and *in silico* ADMET studies of five derivatives. J Mol Struct. 2023;1294:136546. https://doi.org/10.1016/j.molstruc.2023.136546

45. Prasana JC, Muthu S, Abraham CS. Molecular docking studies, charge transfer excitation and wave function analyses (ESP, ELF, LOL) on valacyclovir: A potential antiviral drug. Comput Biol Chem. 2019;78:9-17. https://doi.org/10.1016/j.compbiolchem.2018.11.014

46. Lefi N, Kazachenko AS, Raja M, Issaoui N, Kazachenko AS. Molecular structure, spectral analysis, molecular docking and physicochemical studies of 3-bromo-2-hydroxypyridine monomer and dimer as bromodomain inhibitors. Molecules. 2023;28(6):2669. https://doi.org/10.3390/molecules28062669

47. Demirpolat A, Akman F, Kazachenko AS. An experimental and theoretical study on essential oil of *Aethionema sancakense*: Characterization, molecular properties and RDG analysis. Molecules. 2022;27(18):6129. https://doi.org/10.3390/molecules27186129

Additional information

Peer review: Publisher thanks Sectional Editor and the other anonymous reviewers for their contribution to the peer review of this work.

Reprints & permissions information is available at https://horizonepublishing.com/journals/index.php/PST/open_access_policy

Publisher's Note: Horizon e-Publishing Group remains neutral with regard to jurisdictional claims in published maps and institutional affiliations.

Indexing: Plant Science Today, published by Horizon e-Publishing Group, is covered by Scopus, Web of Science, BIOSIS Previews, Clarivate Analytics, NAAS, UGC Care, etc
See https://horizonepublishing.com/journals/index.php/PST/indexing_abstracting

Publisher information: Plant Science Today is published by HORIZON e-Publishing Group with support from Empirion Publishers Private Limited, Thiruvananthapuram, India.